INTERNATIONAL JOURNAL OF NUMERICAL METHODS IN FLUIDS, VOL. 20, 541–557 (1995)

# MODELLING OF SINGLE SHOT INDUCTION HEATING BY INVERSE FINITE ELEMENT METHOD

G. MAIZZA

*Dipartimento di Scienza dei Materiali ed Ingegneria Chimica, Politecnico di Torino, C.so Duca degli Abruzzi N. 24, 10129, Torino, Italy*

M. CALÌ

*Dipartimento di Energetica, Politecnico di Torino, C.so Duca degli Abruzzi N. 24, 10129, Torino, Italy*

## SUMMARY

The induction heating model described herein couples the standard heat conduction equation with electromagnetic proximity-skin equations. An Inverse Finite Element procedure, which is based on prior *deterministic* and *probabilistic* concepts, has been designed to solve the inherent inverse equation model with respect to the unknown coil current parameter. Simulated experiments using different noises in the input data have been performed in order to determine their influence on the estimated parameter. The IFEM has shown its capability to predict the optimal location for the temperature sensors, together with their numbers, consistently with a pre-specified estimate accuracy. Specifically, only one temperature sensor, located in the middle of the two turns of the coil, results to be sufficient to estimate the unknown parameter to a satisfactory accuracy degree. This, may significantly help to design optimal experiments.

KEY WORDS: electromagnetic induction heating; inverse method; finite element; coupled fields; experiment simulation

## 1. INTRODUCTION

Induction heating of material is extensively used because of its great flexibility in industrial applications. The main feature of induction heating is to keep the size and the shape of the heated zone under control. This is especially important for the heat treatment of specific regions of complex workpieces with high irregular boundaries. As with other similar heating processes, induction heating is also conveniently used thanks to its repeatability properties, its relatively low-energy consumption and its negligible pollution emission.

The optimization of such processes usually requires an analysis of several working parameters and an accurate control of the most critical ones. This analysis may be accomplished experimentally or more economically with the use of specifically designed computational codes. Several rather effective computational techniques are currently available, among these the finite element method seems to be one of the most versatile for solving complex problems. In fact, irregular geometries and strong non-linearities in the partial differential equations may be handled without considerable supplemental efforts.

From a physical point of view, a general and rigorous induction heating model requires the analysis of several coupled fields, such as the thermal, the magneto electric, the mechanical, the micro-structural and the diffusion of the alloying elements of the material being processed. These fields are strongly coupled through their dependence on material properties, boundary conditions

CCC 0271–2091/95/060541–17

*Received 12 February 1994*
*Revised 2 November 1994*

and inductive source. A few field coupling models have been previously examined and solved[1,2] as a deterministic (or direct) problem, according to the definition given by Beck.[3] Other more simplified models have been proposed[4,5] following the same approach, which are based on heat conduction and Maxwell's time-harmonic equations coupling. Except for simple mono-dimensional problems, such models appear significantly costly in terms of memory allocation and execution times especially when applied to on-line simulations. This is mainly due to the complex and intrinsic strong coupled nature of Maxwell's equations which yet need to be integrated not only into the workpiece but also in the surrounding air space.

All these drawbacks have encouraged the authors to search for a more effective induction heating model.

In previous works[6,7] attempts have been made to the model induction heating problem by coupling the electromagnetic proximity-skin model with the heat conduction equation.[8] As a result only the thermal and current density fields need to be computed simultaneously, thus avoiding the non-essential and costly calculation of the magnetic field. When dealing with simple geometries, the proximity-skin effect may be described by a simple equation that is a function of two unknown parameters, i.e. the coil current and the coil–workpiece coupling, respectively. The coil current parameter directly affects the maximum temperature of the cycle. The coupling parameter is basically used for post calculations, for instance, in the estimation of the heating process efficiency. Both these parameters are of fundamental importance for induction heating equipment design and process optimization. However, these parameters are not easy to measure practically, therefore an inverse procedure[6,7] is necessary to solve the inherent parameter estimation problem. In previous works,[6,7] however, no information on the accuracy of the parameter estimation was reported due to the lack of available experimental data.

The aim of this work is to investigate the performance of the inverse procedure adopted in[6,7] with respect to the estimation of the unknown coil current parameter. The choice of the study of such parameter is suggested by the great interest that it covers in practical applications.

Simulated experiments are carried out in order to investigate the influence of the amount of data used as input for the model and the noise effect (if any) on the convergence procedure of the adopted Inverse Finite Element Model (IFEM). The validation of the IFEM has been accomplished by comparisons with both real temperatures and coil current measurements.

## 2. THE PHYSICAL PROBLEM

The system investigated, shown in Figure 1, is arranged vertically. It consists of a cylindrical bar, longitudinally fixed while rotating about its axis to allow for a uniform heating. A two-turn coil,

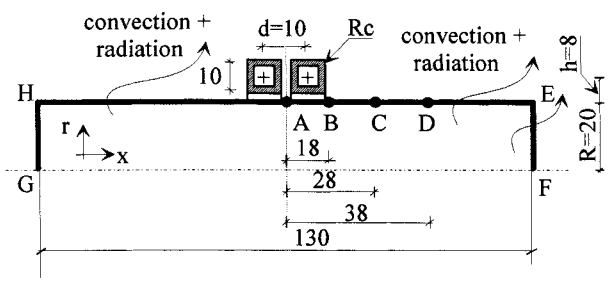


Figure 1. Scheme of the analyzed induction system. For clarity the figure is out of scale. The dimensions indicated are in mm

which is mounted coaxial to the bar, is cooled internally by water and crossed externally by an AC current. The current induces an electromagnetic field on the workpiece causing the rapid heating by a mechanism which is assumed to be governed by the proximity-skin effect theory. The relative position of the coil, with respect to the bar, is assumed to be unchanged during the thermal cycle (single shot heating). The bar, which is surrounded by still air, is cooled by convection (line EF) and by convection–radiation (line HE). A fixed temperature boundary condition is assumed to be applied on the upward cylinder base (line HG).

## 3. THE PROXIMITY-SKIN MODEL

The proximity-skin effect theory[3] was originally derived for a monofilamentary-thin plate conductor system. This theory has been suitably extended to axisymmetric geometries and multi-turn coils.[13] The electromagnetic field generated by the coil directly affects the current density distribution in the workpiece. According to the proximity theory, a single-turn coil causes a surface current density $J_R(x)$ on the workpiece which is distributed along the $x$-axis as

$$J_R(x, I) = \frac{I}{\pi h}\left[1 + \left(\frac{x}{h}\right)^2\right]^{-1} \frac{1}{\text{width}} \tag{1}$$

From equation (1), the dependence of the coil current $I$ and the distance between the coil and the workpiece $h$ on $J_R(x)$ is clear (see Figure 1). If the coil is mounted close to the workpiece, as in actual cases, then the *vicinity effect* has also to be taken into account. In such case a correction $h' = \sqrt{h^2 - R_c^2}$ for $h$ has to be introduced into equation (1), therefore giving

$$J_R(x, I) = \frac{I}{\pi h}\sqrt{1 - \left(\frac{R_c}{h}\right)^2} \cdot \left[1 - \left(\frac{R_c}{h}\right)^2 + \left(\frac{x}{h}\right)^2\right]^{-1} \frac{1}{\text{width}} \tag{2}$$

Where $R_c$ is the radius of the coil cross-section. With only the purpose of evaluation the power distribution in the workpiece in mind, it has been shown[13] that equation (2) can be extended with satisfactory approximation, to any cross-section shape, provided the radius $R_c$ is replaced by an equivalent one. In the present work, the equivalent radius $R_c$ has been deduced by comparing the total current flowing into the actual (square) coil cross-section with that flowing into an imaginary round one of a size $R_c$, and solving the equation with respect to the equivalent $R_c$.

For a correct estimation of the coil current $I$, it is necessary that such a calculation be accomplished till the end of the heating process in order to obtain a more reliable and representative mean value of $I$ over the whole cycle.

In addition, the superposition principle is applied to all the turns that compose the coil in order to take all the individual current density effects at each integration point of the heat-treated material[11] into account. As a result, the following equation is derived in the case of a double-turn coil system:

$$J_R(x, I) = \frac{I}{\pi h}\left\{\left[1 + \left(\frac{x - d/2}{h}\right)^2\right]^{-1} + \left[1 + \left(\frac{x + d/2}{h}\right)^2\right]^{-1}\right\} \frac{1}{\text{width}} \tag{3}$$

where $d$ is the inter-distance of the two turns.

From the same theory, the surface power density peak, $\text{PD}_{\text{MAX}}$, given by

$$\text{PD}_{\text{MAX}} = \frac{\rho_s}{\delta}\left[\frac{I}{\pi h}\right]^2 \tag{4}$$

which determines the maximum temperature of the cycle $T_{\text{MAX}}$.

In equation (4), the symbol $\delta$ represents the skin depth (defined in equation (8)), and $\rho_s$ is the electrical resistivity of the workpiece.

For axisymmetric geometries the width in (1)–(3) is simply replaced by $2\pi R$.

An auxiliary empirical equation (8) for the power density is given by

$$\mathrm{PD}_{\mathrm{MAX}} = \frac{\vartheta_m R \rho c}{2\tau_{\mathrm{H}}} \tag{5}$$

with

$$\vartheta_m = T_{\mathrm{MAX}} - T_a \tag{6}$$

where $R$, $\rho$, $c$ are the radius, the density, and the specific heat of the workpiece respectively, while $\tau_{\mathrm{H}}$ is the heating time.

Numerical experience has shown that equations (4) and (5), when solved with respect to $I$, provide a good starting value for initiating the iterative procedure in the Inverse finite element model.

Finally, the skin effect theory provides the current density distribution in the bulk as a function of the workpiece radius $r$:

$$\frac{J(r,x,I)}{J_R(x,I)} = \frac{\mathrm{ber}'(\sqrt{2r/\delta}) + \mathrm{j}\,\mathrm{bei}'(\sqrt{2r/\delta})}{\mathrm{ber}'(\sqrt{2R/\delta}) + \mathrm{j}\,\mathrm{bei}'(\sqrt{2R/\delta})} \tag{7}$$

In equation (7), ber′ and bei′ are the derivatives of the functions, named by Kelvin, to express, respectively, the real part and the imaginary part of the Bessel functions. The well-known equation for determining the skin depth is

$$\delta = (\rho_s/\pi\mu f)^{0.5} \tag{8}$$

where $\mu$ is the magnetic permeability and $f$ is the service frequency.

The overall current density distribution $J(r,x,I)$ is easily found by combining equations (3) and (7). In the present study all the material properties, including the source term $q_v$ are, at least, temperature dependent. The inductive heat generation rate per unit of volume is

$$q_v(r,x,I) = \rho_s |J(r,x,I,T)|^2 \tag{9}$$

The peculiarity of the present proximity-skin model, with respect to the Maxwellian one, is that the end physical effect, (i.e. the current density distribution), in the workpiece is easily available for the subsequent calculation of the power density distribution without any need to precalculate the magnetic field. This will contribute to a significant saving of memory requirements.[13] Furthermore, it has been shown[12] that such a electromagnetic model, when applied in conjunction with finite elements, provides a good estimation of the power distribution and the net power supplied to the workpiece with respect Maxwell's equation model.

## 4. THE THERMAL MODEL

The standard heat conduction equation, written in tensor notation, is

$$[k(T)T_{,i}]_{,i} + q_v(r,x,I,T) = \rho c(T)\partial_t T \tag{10}$$

with $k$ the thermal conductivity of the workpiece.

The boundary conditions are of the Newton type on the downward base EF and on the lateral surface HE as shown in Figure 1:

$$-k(T)T_{,i} = \alpha(T - T_a) + \sigma\varepsilon(T^4 - T_a^4) \tag{11}$$

In equation (11) $\alpha$ is the convection coefficient for still air, $\varepsilon$ is the surface emissivity of the workpiece and $\sigma$ the Stefan–Boltzmann constant. The prescribed temperature boundary condition (on the upward base HG) is given by

$$T(r, -L/2, t) = T_a \tag{12}$$

The initial condition is

$$T(r, x, 0) = T_a \tag{13}$$

## 5. THE INVERSE PROBLEM

A general physical problem may be modelled by a minimum set of quantities defined as *model parameters*.[3] Some of these quantities, designated as *model data* **d**, have the property of being measurable; other quantities designated as *model parameters* **m**, are not measurable. A general model may be written as

$$F(\mathbf{d}, \mathbf{m}) = 0 \tag{14}$$

To solve the problem (14) two approaches are possible, either a *direct* or an *inverse* one. In the *direct model*, equation (14) is solved in the following generic functional form:

$$\mathbf{d} = G(\mathbf{m}) \tag{15}$$

in which the measurable quantities **d** are calculable provided that the non-measurable **m** are known. This is normally done, for instance, in cases where the temperatures are calculated by FEM, starting from the prior knowledge of thermophysical properties and boundary/initial conditions. This type of problem has been extensively solved in the past in many engineering fields.[1,2,4]

In the *inverse model*, equation (14) is solved in the form

$$\mathbf{m} = G^{-1}(\mathbf{d}) \tag{16}$$

where, the non-measurable quantities **m** are calculated from the prior knowledge of the measurable data **d**. The inverse approach has been successfully applied in a few engineering fields[3,9] since it allows the evaluation of the system features with the aid of measurements. However it has the disadvantage of adding new experimental uncertainties or experimental errors to the ordinary mathematical model. Due to this, models of inverse type have to rely on mixed *deterministic* and *probabilistic* concepts.

The methods proposed by Beck for the analysis of heat conduction problems[3] and by Tarantola[9] for the analysis of geological problems are here adopted to solve the parameter estimation problem. Before going into details on the IFEM, some definitions are necessary.

In this work the measurable data **d** is replaced with a set of observed temperatures **Y**, defined as

$$\mathbf{Y}^T = [\mathbf{Y}_1^T \cdot\cdot \mathbf{Y}_j^T \cdot\cdot \mathbf{Y}_M^T]^T \tag{17}$$

where each element corresponds to the $m$th spatial point located on the surface (as A, B, C, and D shown in Figure 1). The non-measurable quantity **m** is represented by the unknown coil current parameter $I$.

For the $j$th element of **Y**, $N$ discrete components representing $N$ observations in time are defined. The resulting **Y** vector contains $N$ by $M$ elements:

$$\mathbf{Y}_j^T = \mathbf{Y}^T(t_j) = [Y_1(t_j) \cdot\cdot Y_i(t_j) \cdot\cdot Y_N(t_j)]^T \tag{18}$$

Analogously, a vector $\hat{\mathbf{T}}$, which is referred to the calculated temperatures evaluated to the same $M$ points and $N$ sampling times, is defined as

$$\hat{\mathbf{T}}^{\mathrm{T}} = [\hat{\mathbf{T}}_1^{\mathrm{T}} \cdot\cdot \hat{\mathbf{T}}_i^{\mathrm{T}} \cdot\cdot \hat{\mathbf{T}}_M^{\mathrm{T}}]^{\mathrm{T}} \tag{19}$$

where

$$\hat{\mathbf{T}}_j^{\mathrm{T}} = \hat{\mathbf{T}}^{\mathrm{T}}(t_j) = [\hat{T}_1(t_j) \cdot\cdot \hat{T}_i(t_j) \cdot\cdot \hat{T}_N(t_j)]^{\mathrm{T}} \tag{20}$$

In the following, we assume that the material properties, the boundary conditions and all the working parameters (except $I$) in the mathematical model are known. Then the measured and the calculated temperatures differ ideally by some quantity that depends on both the measurement and the model representation errors. To account for such differences two quantities are introduced, namely the *residual*:

$$\mathbf{s}(I) = \hat{T}(I) - \mathbf{Y} \tag{21}$$

and the *experimental error*:

$$\mathbf{e} = \mathbf{Y}_{\mathrm{e}} - \mathbf{Y} \tag{22}$$

In equation (22), $\mathbf{Y}_{\mathrm{e}}$ are the *true* (exact) observed values, while $\mathbf{Y}$ are those measured by instruments. Since it is practically impossible to know $\mathbf{Y}_{\mathrm{e}}$ exactly it will be replaced by the numerical values $\mathbf{T}(I)$ which may be provided by using a reliable computational model. Accordingly, the errors $\mathbf{e}$ may be replaced by the residuals $\mathbf{s}$.

According to Tarantola,[9] it has been assumed that the residuals hold a normal (Gaussian) distribution, with zero mean and standard deviation $\sigma$ known. Therefore, the probability density of the unknown parameter $I$ may be expressed in the generic form as

$$\psi(I) = K \exp[-\tfrac{1}{2} S(I)] \tag{23}$$

Here, $K$ is a suitable constant, while $S(I)$ is a function of the square residuals defined by

$$S(I) = \mathbf{s}^{\mathrm{T}} \mathbf{C}_{\mathrm{e}}^{-1} \mathbf{s} = [\hat{\mathbf{T}}(I) - \mathbf{Y}]^{\mathrm{T}} \mathbf{C}_{\mathrm{e}}^{-1} [\hat{\mathbf{T}}(I) - \mathbf{Y}] \tag{24}$$

where $\mathbf{C}_{\mathrm{e}}$ is the square symmetric covariance matrix of the residuals.

If the measurement errors are still assumed uncorrelated, the covariance matrix $\mathbf{C}_{\mathrm{e}}$ reduces to the main diagonal matrix, where each element is equal to the standard deviation of the related measurement data:

$$\mathbf{C}_{\mathrm{e}} = \mathrm{diag}[\sigma_1^{-2}, \sigma_2^{-2}, \ldots, \sigma_{NM}^{-2}] \tag{25}$$

It can be shown that an optimal estimation of parameter $I$ may be obtained by minimizing the function $\psi(I)$ in equation (23) with respect to $I$.

Tarantola[9] demonstrates that it is possible to adequately describe the probability density of the unknown parameter $I$ by calculating the point of maximum likelihood. This may be obtained by searching for the maximum of equation (23), or by searching for the minimum of equation (24), with respect to the parameter $I$, that is to say

$$\mathrm{d}S = \frac{\mathrm{d}S}{\mathrm{d}I}\,\mathrm{d}I = 2\mathbf{X}^{\mathrm{T}} \mathbf{C}_{\mathrm{e}}^{-1} [\hat{\mathbf{T}}(I) - \mathbf{Y}] \mathrm{d}I = 0 \tag{26}$$

where $\mathbf{X}$ is the sensitivity coefficients vector defined as

$$\mathbf{X} = \frac{\mathrm{d}\hat{\mathbf{T}}(I)}{\mathrm{d}I} \tag{27}$$

However, since $S$ depends on $I$ through a non-linear relationship, an iterative procedure is required.

If $\tilde{I}$ is an estimate of $I$, then the model values $\hat{T}$ may be obtained by linearization about the parameter $I$ in its neighbourhood:

$$\hat{\mathbf{T}}(I) = \hat{\mathbf{T}}(\tilde{I}) + \mathbf{X}(I - \tilde{I}) \tag{28}$$

If equation (28) is substituted in equation (23) the following non-linear equation system will result:

$$\mathbf{X}^{\mathrm{T}}\mathbf{C}_{\mathrm{c}}^{-1}[\hat{\mathbf{T}}(\tilde{I}) + \mathbf{X}\cdot(I - \tilde{I}) - \mathbf{Y}] = 0 \tag{29}$$

The solution of equation (29) can be achieved numerically by applying the following iterative scheme:

$$I^{(k+1)} = I^{(k)} + P^{-1}(I)^{(k)}\cdot H(I)^{(k)} \tag{30}$$

where

$$\begin{aligned} P^k &= \mathbf{X}^{\mathrm{T}}(I^k)\cdot\mathbf{C}_{\mathrm{c}}^{-1}\cdot\mathbf{X}(I^k) \\ H^k &= \mathbf{X}^{\mathrm{T}}(I^k)\cdot\mathbf{C}_{\mathrm{c}}^{-1}\cdot[\hat{\mathbf{T}}(I^k) - \mathbf{Y}] \end{aligned} \tag{31}$$

The parameter $I^{(k+1)}$ is updated at each iteration until a suitable convergence criterion is satisfied:

$$|I^{(k+1)} - I^{(k)}|/|I^{(k)}| \leqslant \mathrm{tol} \tag{32}$$

with tol being a suitable pre-defined tolerance value.

At the end of the iteration process, either the standard deviation ($\sigma_I^2$) or the variance of the parameter estimated ($\sigma_I$) may be computed as a measure of the accuracy of the estimation procedure.

The former is given by

$$\sigma_I^2 = \mathbf{X}^{\mathrm{T}}(I_{ML})\cdot\mathbf{C}_{\mathrm{c}}^{-1}\cdot\mathbf{X}(I_{ML}) \tag{33}$$

where $I_{ML}$ is the unknown parameter estimated by the maximum likelihood approach.

Finally, the index used as a measure of the accuracy for modelling induction heating experiments may be defined as[3]

$$\sigma_{\mathrm{T}}^2 = \frac{\mathbf{X}^{\mathrm{T}}(I_{ML})\mathbf{X}(I_{ML})}{(NM)} \tag{34}$$

## 6. THE INVERSE-FE MODEL

In induction heat treatment problems the material may undergo phase changes which greatly influence the problem solution. In the present case this problem has been avoided by choosing an aluminium alloy which does not change its crystallographic structure before the melting temperature.

From equations (10) and (11) the following well-known FE equation set is derived:

$$\mathbf{C}(\mathbf{T})\dot{\mathbf{T}} + \mathbf{K}(\mathbf{T})\mathbf{T} + \mathbf{F}(\mathbf{T}, I) = \mathbf{0} \tag{35}$$

where **C**, **K**, **F** are the capacity matrix, the stiffness matrix and the load term vector, respectively.

These arrays are defined as follows:

$$C_{ij} = \sum_e \int_{V^e} \rho c N_i N_j \, \mathrm{d}V^e \tag{36}$$

$$K_{ij} = \sum_e \int_{V^e} \left[ k_r(T) \frac{\partial N_i}{\partial r} \frac{\partial N_j}{\partial r} + k_x(T) \frac{\partial N_i}{\partial x} \frac{\partial N_j}{\partial x} \right] \mathrm{d}V^e + \sum_e \int_{S^e_{EF}} \bar{\alpha} N_i N_j \, \mathrm{d}S^e + \sum_e \int_{S^e_{HE}} \bar{\alpha} N_i N_j \, \mathrm{d}S^e \tag{37}$$

$$F_{ij} = -\sum_e \int_{S^e_{EF}} \alpha N_i T_a \, \mathrm{d}S^e - \sum_e \int_{S^e_{HE}} \bar{\alpha} N_i T_a \, \mathrm{d}S^e + \sum_e \int_{V^e} q_v(I, T) N_i \, \mathrm{d}V^e \tag{38}$$

Matrices **C** and **K** are temperature dependent only. The effective convection–radiation coefficient is defined as

$$\bar{\alpha} = \alpha + \sigma \varepsilon (T_s + T_a)(T_s^2 + T_a^2) \tag{39}$$

The system (35) has to be solved in an inverse manner, due to the fact that temperatures are measured at some points and vector **F** is dependent on both **T** and $I$, through $q_v$. Equation (10) has been integrated in space by using four-node quadrilateral isoparametric finite elements. The so-called single-step first-order predictor–corrector recurrence scheme (SS11) has been used to integrate the set (35) of ordinary differential equations.[10] The algorithm allows an automatic timestep selection during time integration, based on the control of the local time truncation error.[10]

The computational steps of the IFEM are summarized in the algorithm of Figure 2.

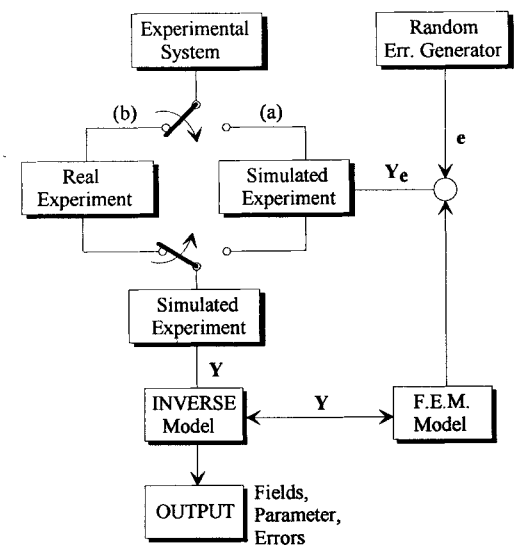


Figure 2. Inverse finite element model algorithm used for the solution of the unknown parameter estimation in induction heating problems

## 7. RESULTS AND DISCUSSION

In order to simplify the following numerical tests an axisymmetric geometry has been investigated, though the model may be applied to more complex configurations.

The IFEM is first applied to analyse how different measurement noise levels may affect the estimated parameter. This question generally arises in optimal experiment design problems when one has to select the most suitable instrument class compatibly with the prefixed target accuracy. To pursue this objective two paths are possible, (a) or (b), as shown in Figure 3. The main difference between each path is the origin of the data source. Frequently, data comes from laboratory experiments that are performed on real systems (i.e. path a). An alternative is to generate them by simulated experiments (i.e. path b).

Path (a) is first considered. Initially, a hypothetical *true value*, namely $I = 4920$ A, is assumed for the coil current. This current value is consistent with actual measurements performed during heating at 6 kHz. The boundary conditions that completely define the thermal problem are schematically shown in Figure 1. Specifically, they are of three types: (a) prescribed, with temperature set at 25°C on side HG; (b) convection and radiation in air, on the lateral surface HE; (c) convection in air, on the bottom base of the cylinder EF. The mean convection coefficient $\alpha$ has been set to 30 W/m$^2$ K, while the surface emissivity has been set at a constant value equal to 0·7. The initial temperature of the material is assumed to be equal to 25°C, which corresponds to the equilibrium temperature of the surrounding environment. The cycle duration is equal to 6 s. The material properties, (i.e thermal conductivity $k$, specific heat $c$, the electrical resistivity $\rho_s$ and the density $\rho$) for the given material (i.e. aluminium alloy) are assumed to be variable with the temperature[8] (see Table I).

1. *Set problem data and boundary/initial conditions*
2. *Initialize counters* $k = 0$; *set initial parameter* $I^0$, $\Delta I^0 = 0$
3. *Increment parameter iteration counter* $k = k + 1$
   *Update parameter* $I^k = I^{k-1} + \Delta I^{k-1}$ *(see eq.*
4. *loop* $j = 0$ *to 1 - solve following 5-12 steps twice (*)*
5. *Update parameter* $I^k = I^k + j \cdot dI^k$
6. *Initialize time loop:* $t_0 = 0$, $n = 0$
7. *Increment time counter:* $n = n + 1$
   *Increment time step* $t_n = t_{n-1} + \Delta t_n$
8. *Update electrical- magnetic properties* $\rho_s(\hat{\mathbf{T}}^{n-1}), \mu(\hat{\mathbf{T}}^{n-1})$
9. *Compute electric density field* $\hat{\mathbf{J}}(r,z)^n$, *and* $q_v(\hat{\mathbf{J}})^n$
10. *Update thermal properties* $k(\hat{\mathbf{T}}^{n-1}), \rho c(\hat{\mathbf{T}}^{n-1})$
11. *Solve for the thermal field* $\hat{\mathbf{T}}(r,z)^n$
12. *If* $t_n < \tau_H$ *go to 7*
13. *Increment j*
14. *Compute H, P, X, S,* $C_C$
15. *Check for parameter convergence, if fulfilled go to 17*
16. $\Delta I^k = P^{-1}(I^k) \cdot H(I^k)$ and *go to 3*
17. *Print Output: I;* $\hat{\mathbf{J}}(r,z)$; $\hat{\mathbf{T}}(r,z)$; $\sigma_T$, $\sigma_I$
18. *END*

Figure 3. Scheme for optimal experiment design

Table I. Material properties for the aluminium alloy used in the calculations

| $T$ (°C) | $\rho_s$ ($\Omega$ m) | $\rho c$ (W s m$^{-3}$ K$^{-1}$) | $k$ (W m$^{-1}$ K$^{-1}$) |
|---|---|---|---|
| 20 | $0{\cdot}027 \times 10^{-6}$ | $2{\cdot}52 \times 10^{6}$ | 211 |
| 100 | $0{\cdot}0364 \times 10^{-6}$ | $2{\cdot}59 \times 10^{6}$ | 219 |
| 200 | $0{\cdot}0478 \times 10^{-6}$ | $2{\cdot}65 \times 10^{6}$ | 224 |
| 300 | $0{\cdot}0599 \times 10^{-6}$ | $2{\cdot}71 \times 10^{6}$ | 223 |
| 400 | $0{\cdot}073 \times 10^{-6}$ | $2{\cdot}78 \times 10^{6}$ | 216 |
| 500 | $0{\cdot}087 \times 10^{-6}$ | $2{\cdot}84 \times 10^{6}$ | 209 |
| 600 | $0{\cdot}104 \times 10^{-6}$ | $2{\cdot}89 \times 10^{6}$ | 200 |

The finite element solver is first executed in a direct fashion (i.e. in one iteration) in order to provide the overall temperature field for the workpiece $\{T\}$. Special care has been taken to design the mesh near the surface, within the skin depth region, where high-temperature gradients are to be expected. Prior tests have suggested that a non-uniform mesh of 153 nodes and 128 elements is an optimal trade-off between calculation accuracy and execution times. The average (stationary) timestep used for time integration has been of about 0·01 s, except for the early stage of the transient in which it has been reduced to an order of $1 \times 10^{-4}$ s.

Conventionally, the temperatures obtained by the finite element model at this step are designated as '*exact*' $\mathbf{Y}_e$. From the nodal solution vector $\mathbf{Y}_e$ a subset of $NM$ ( $= 7 \times 4$) sample values has been extracted. These values correspond to fictitious temperature readings made at $N$ specified space locations along the surface (points A, B, etc. in Figure 1) and $M$ discrete sampling times. Then, three sets of random temperature errors of variance $\sigma_{SIM}$ (4, 5, 15°C, respectively) are generated by the computer[3] and added to $\mathbf{Y}_e$. As a result three vectors $\mathbf{Y}$ are obtained as input data for the IFEM. These data are subsequently used to investigate the influence of random errors on the estimated parameter. Cases from A1 to A5 and A7 are solved by the Ordinary Least Square method (OLS), which means that all the main diagonal terms of the covariance matrix $\mathbf{C}_c$ are set to one. In this way, the experimental errors are not taken into account. About four iterations are necessary to achieve the final solution. The sixth column in Table II (tests A1–A3) shows that the maximum likelihood parameter can be estimated within a spread of about $\pm$ 30 A. The two accuracy indexes $\sigma_I$ and $\sigma_T$ are provided in the seventh and eighth column, respectively. As already mentioned, the former gives the accuracy associated to the estimation procedure, the latter represents the *goodness index* of the temperature fitting. Figures 4–6 show the results from the best-fit analysis performed for the test cases A1, A2, A3, respectively.

Further tests, A4–A8, show how the amount of input information entered into the model influences the parameter estimation accuracy. Furthermore, these tests are carried out to check whether IFEM is sensitive to spatial or temporal data and how data may affect the convergence process. In the case A4, only $N = 7$ time records at $M = 1$ points (i.e. point A) are considered. The importance of point A is due to the fact that it corresponds to the location of the maximum temperature in the cycle. In this case A5, data at only $N = 3$ time levels are taken into account (i.e. the initial, the final and an intermediate one) at $M = 4$ points (i.e. A, B, C and D). The results of fitting for the cases A4 and A5 are shown in Figures 7 and 8, respectively. Case A6 is aimed at investigating on the estimation behaviour when experimental error information is also introduced as input to the IFEM. For this purpose a Weighted Least Squares (WLS) model, with a suitable covariance matrix $\mathbf{C}_c$ is constructed. According to equation (25), the diagonal of the

Table II. Coil current estimates obtained using simulated temperature data (A) and real recorded temperatures (B) during induction heating at 8 kHz and duration of 12 s

| Test | $NM$ | $f$ (kHz) | $\tau_H$ (s) | Meth. | $\sigma_{SIM}$ (°C) | $I$ (A) | $\sigma_I$ (A) | $\sigma_T$ (°C) |
|---|---|---|---|---|---|---|---|---|
| A0 | 28 | 6 | 6 | Exact | 0 | 4920 | 0 | 0 |
| A1 | 28 | 6 | 6 | OLS | 5 | 4891 | 2·5 | 5·5 |
| A2 | 28 | 6 | 6 | OLS | 15 | 4900 | 3 | 10·5 |
| A3 | 28 | 6 | 6 | OLS | 4 | 4910 | 2 | 4·5 |
| A4 | 7 | 6 | 6 | OLS | 5 | 4891 | 3·5 | 5 |
| A5 | 12 | 6 | 6 | OLS | 5 | 4924 | 3 | 3·5 |
| A6 | 28 | 6 | 6 | WLS | 5 | 4920 | 2 | 2·5 |
| A7 | 2 | 6 | 6 | OLS | 5 | 4893 | 4 | 4·5 |
| A8 | 2 | 6 | 6 | WLS | 5 | 4891 | 4 | 3 |
| B1 | 36 | 8 | 12 | OLS | — | 3966 | 1·0 | 16 |
| B2 | 36 | 8 | 12 | WLS | — | 3961 | 6·0 | 15 |

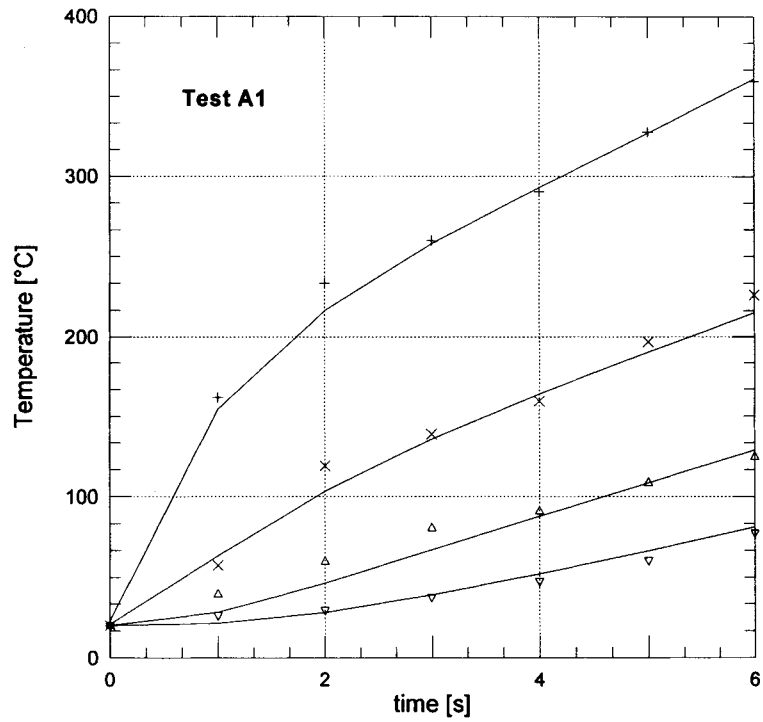


Figure 4. Matching between simulated (symbol) and model (line) temperatures in the case of $\sigma_{SIM} = 5$°C. The simulation refers to an induction heating process performed at 6 kHz for 6 s on aluminium alloy

covariance matrix is here filled with values that mimic the instrument accuracy at the various temperature levels. In actual laboratory experiments, an optical fibre pyrometer has been used for recording temperatures at $T \geqslant 300$°C with satisfactory accuracy. However, the range of temperature $T < 300$°C have been measured using a contact thermometer with inherent inaccuracy

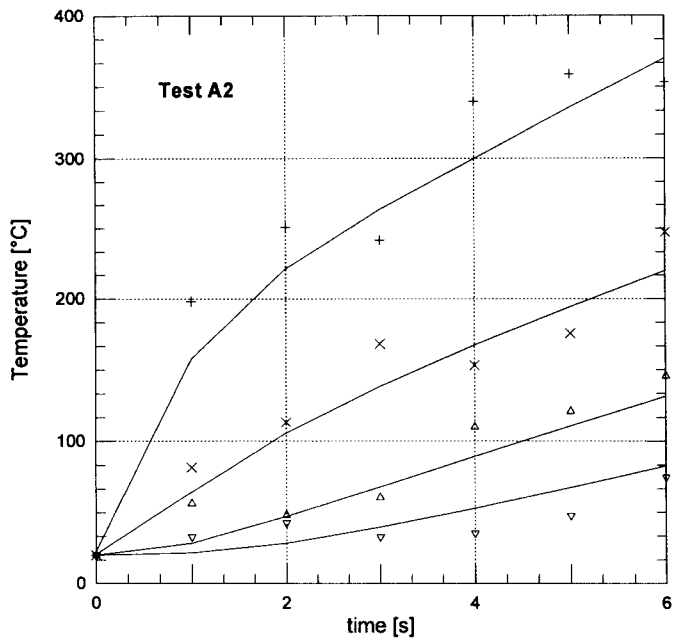


Figure 5. Matching between simulated (symbol) and model (line) temperatures in the case of $\sigma_{SIM} = 15°C$. The simulation refers to an induction heating process performed at 6 kHz and heating time equal to 6 s on aluminium alloy

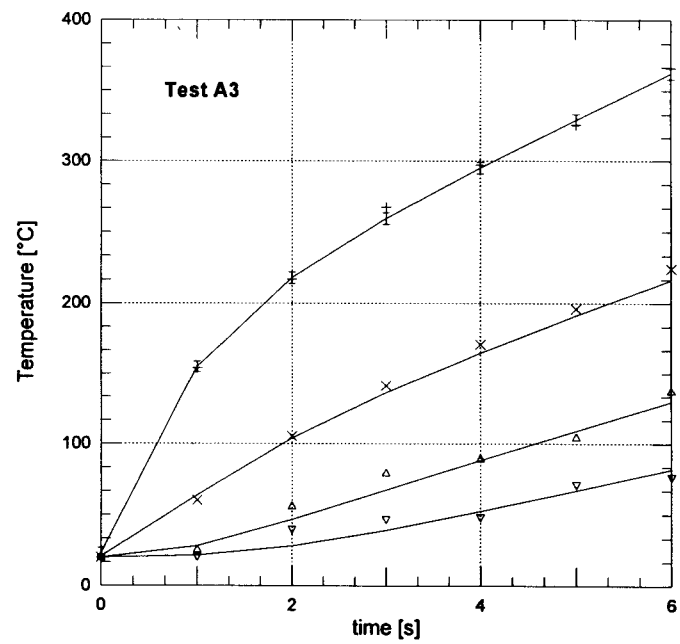


Figure 6. Matching between simulated (symbol) and model (line) temperatures in the case of $\sigma_{SIM} = 4°C$. The simulation refers to an induction heating process performed at 6 kHz and heating time equal to 6 s on aluminium alloy

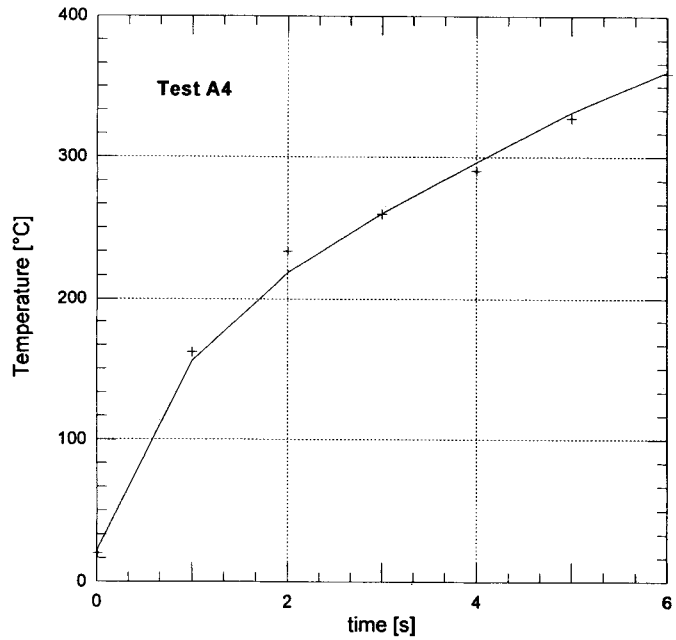


Figure 7. Matching between simulated (symbol) and model (line) temperatures in the case of a reduced amount of input data. Temperatures are recorded at 7 time instants at the point located in the middle of the two turns of the coil (i.e. A)

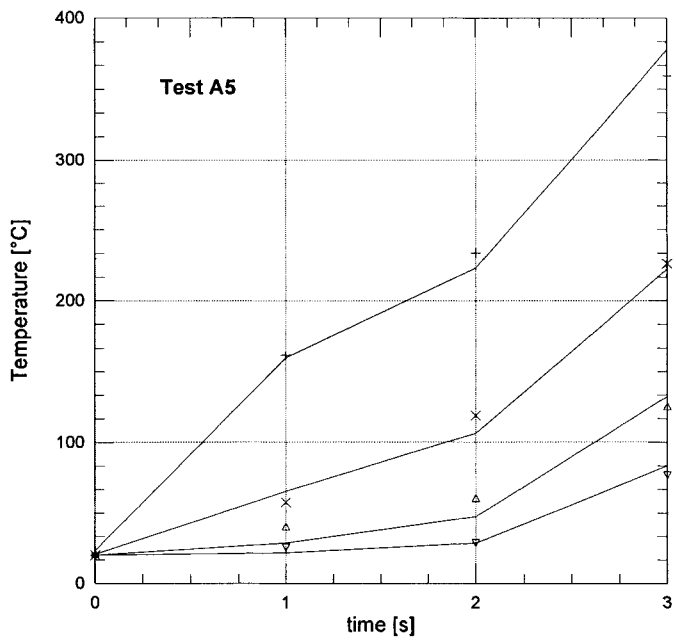


Figure 8. Matching between simulated (symbol) and model (line) temperatures in the case of a reduced amount of input data. Temperatures are recorded at 3 time instants at 4 location points of the cylinder surface (i.e. A, B, C and D)

problems. The temperatures in the interval of about 300°C have been taken as average from both the pyrometer and the thermometer measurements. To take these errors into account, relatively low standard deviations have been assigned to those elements of the covariance matrix related to low-temperature data.

The use of the covariance matrix has actually improved the convergence of the IFEM by lowering the number of iterations to four instead of five. Even further improvement may be expected by finer tuning of the diagonal element values of the $\mathbf{C}_c$ matrix. The best-fitting result of the A6 case is not reported here since it much resembles that shown in Figure 4.

As an extreme case, the effect of $M = 1$ spatial point (i.e. A) and $N = 2$ records, i.e. the initial ($t = 0$ s) and the final ($t = \tau_H$) has been investigated with and without the use of the covariance matrix $\mathbf{C}_c$. The results of the A7 and A8 test cases are summarized in Table II.

Examination of columns sixth, seventh and eighth in Table II shows that, even with a low amount of input data, $\sigma_I$ does not increase excessively and the spread of the unknown parameter is within the range of $\pm$ 30 A which is consistent with that observed in real experiments.

In this sense, point A, may be regarded as the most critical location since the parameter estimation procedure is very sensitive to the temperature data measured at this point.

To check the validity of the inverse procedure here proposed, actual coil current measurements have been directly carried out on the experimental system. The coil current measured is about 3930 $\pm$ 30 A, at 8 kHz with a heating cycle of 12 s. The temperature histories have been measured at $M = 4$ locations (i.e. points A, B, C, and D) and $N = 9$ discrete sampling times. The temperature data recorded is given in Table III.

The computational results of the B1 case obtained from the application of IFEM with an OLS estimator are summarized in Table II. The B2 case refers to the same problem but with the use of the covariance matrix $\mathbf{C}_c$. Figures 9 and 10 show the fitting between the experimental temperatures and those calculated using the inverse model. Plate 1 shows the isotherms map at 12 s with a modified aspect ratio for the sake of clarity.

From an examination of Table II, one again finds that the parameter estimated is in quite good agreement with that measured directly on the system. The estimated uncertainty is still of $\pm$ 30 A and is in the range of the experimental errors. In seventh column of Table II, it is confirmed that $\sigma_I$ is bounded in both B1 and B2 cases meaning that the proximity-skin model employed is

Table III. Temperature records in (°C) in the case of aluminium alloy during induction heating at 8 kHz and duration of 12 s

| Heating time (s) | Temperature at location $x$ (°C) | | | |
|---|---|---|---|---|
| | A | B | C | D |
| 0 | 25 | 25 | 25 | 25 |
| 2 | 174 | 75 | 40 | 27 |
| 4 | 250 | 123 | 70 | 44 |
| 6 | 314 | 186 | 105 | 65 |
| 8 | 378 | 225 | 123 | 78 |
| 9 | 397 | 238 | 142 | 87 |
| 10 | 429 | 263 | 161 | 92 |
| 11 | 455 | 289 | 171 | 110 |
| 12 | 474 | 301 | 187 | 139 |

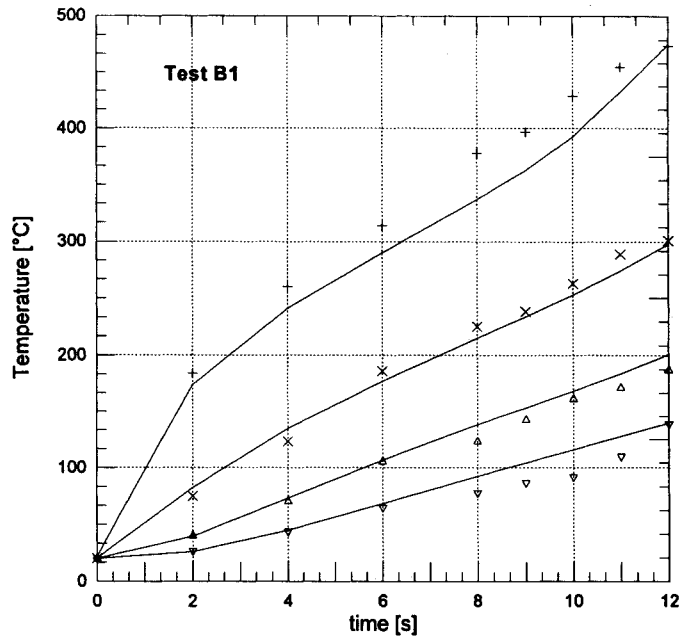


Figure 9. Comparison between experimental (symbol) and model (line) temperatures in the case of an induction heating process performed at 8 kHz for 12 s on aluminium alloy. The inverse model calculations have been carried out using the OLS estimation method

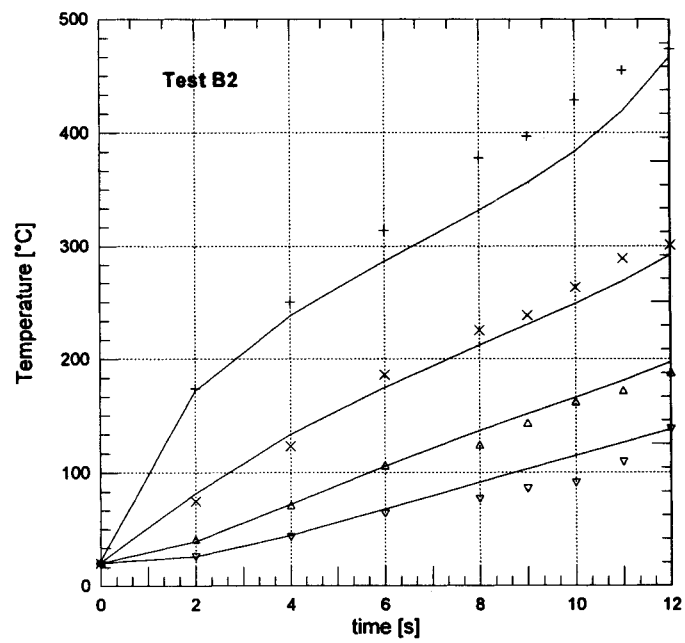


Figure 10. Comparison between experimental (symbol) and model (line) temperatures in the case of an induction heating process performed at 8 kHz for 12 s on aluminium alloy. The inverse model calculations have been carried out using the WLS estimation method

capable of modelling induction heating problems satisfactorily. Furthermore, the IFEM has shown that, as an extreme case, it is possible to estimate the unknown parameter within the limit of the experimental errors by using only one piece of input data, that is the temperature measured at the end of the cycle ($t = \tau_H$) at the point location A. Numerical experiments not shown here[13] demonstrate that the same conclusion cannot be drawn if the A7 and A8 tests consider points such as B, C and D instead of A.

## 8. CONCLUSIONS

The results demonstrate that non-linear transient induction heating problems can be effectively modelled by conduction and proximity-skin equations.

Temperature data is first used to solve the inherent parameter estimation problem. Measurements are easily performed by means of an optical pyrometer that records the thermal histories at specific sensor locations along the workpiece surface during on-line processing.

Simulated experiments show that a good estimation of the coil current parameter can be obtained by a relatively low amount of input data. As an extreme case only one temperature measurement, i.e. in the middle of the coil turns, is enough for a satisfactory estimation of the unknown parameter. The more accurate the measurement of the maximum temperature is, the more reliable is the parameter estimation procedure.

The IFEM has shown its capability to predict the critical location and the optimal number of temperature sensors consistently with a pre-specified estimate accuracy.

From a practical point of view, the present procedure can be applied to a real plant to obtain an on-line control of any desired temperature in the workpiece together with the penetration depth by feed-back monitoring of the coil current.

Finally, the IFEM has been satisfactorily used also when more than one parameter has to be estimated simultaneously. However, in some cases mild instabilities have been observed, probably due to the ill-posed nature of the problem.

## NOTATIONS

| | |
|---|---|
| $c$ | specific heat, J/(kg K) |
| f | working frequency, Hz |
| $h$ | distance between bar and coil, m |
| $H, P$ | working variables |
| $I$ | coil current, A |
| $\tilde{I}$ | guess value for coil current, A |
| $I_{ML}$ | coil current estimated by maximum likelihood criterion, A |
| $J(r)$ | current density at radius $r$, A/m$^2$ |
| $J_R$ | current density at radius $R$, A/m$^2$ |
| $k$ | thermal conductivity, W/(m K) |
| $M$ | number of discrete sample locations |
| $N$ | number of discrete sample times |
| PD | power density per unit of length, W/m$^3$ |
| $q_v$ | internal heat generation rate, W/m$^3$ |
| $S$ | weighted sum of square residuals |
| $t$ | time, s |
| $T$ | temperature, °C |
| $R_c$ | coil radius or an equivalent one, m |

$T_a$ ambient temperature, K
$\alpha$ convection coeff. W/(m$^2$ K)
$\delta$ skin depth, m
$\mu$ magnetic permeability,
$\rho$ density, kg/m$^3$
$\rho_e$ electrical resistivity, $\Omega$/m
$\sigma_I$ estimated current variance, A
$\sigma_T$ variance of $T$ values, °C
$\tau_H$ heating time, s
$\varepsilon$ emissivity
$\tau_H$ heating time, s

*Matrices*

$\mathbf{C}$ capacity matrix
$\mathbf{C}_c$ covariance matrix
$\mathbf{d}$ experimental model data
$\mathbf{e}$ experimental error
$\mathbf{F}$ load vector
$\mathbf{K}$ conductance matrix
$\mathbf{m}$ model parameters
$\mathbf{s}$ residuals
$\mathbf{T}$ temperature vector
$\hat{\mathbf{T}}$ temperatures calculated at the same nodes and times of $\mathbf{Y}$
$\mathbf{Y}$ observed temperatures
$\mathbf{Y}_e$ exact observed temperatures
$\mathbf{X}$ sensitivity coefficients

## REFERENCES


1. M. Melander, 'Computer predictions of progressive induction hardening of cylindrical components', *Mat. Sci. Technol.*, **1,** 877–882 (1985).
2. M. Calì, B. Debenedetti and A. Demiss, 'Non-linear thermal problems in progressive induction hardening', *Proc. AST World Conf. on Advances in Surface Treatment and Surface Finishing*, Paris, 3–4 December 17, 1986.
3. J. V. Beck and K. J. Arnold, *Parameter Estimation in Engineering Science*, Wiley, New York, 1977.
4. J. D. Lavers, 'Numerical solution methods for electro-heat problems', *IEEE Trans. Magn.* **MAG-19,** 2566–2572 (1983).
5. Ch. Marchand and A. Foggia, '2-D Finite element program for magnetic induction heating', *IEEE Trans. Magn.*, **MAG-19,** 2647–2649 (1983).
6. G. Maizza, M. Kitajima and B. Debenedetti, '*FEAHT* A PC-based package for solving coupled problems on induction heat treatments', *Proc. Int. Conf. on Heat and Surface '92*, Kyoto 17–20 November, 1992.
7. B. Debenedetti and G. Maizza, 'Metodo inverso per la risoluzione di problemi di riscaldamento ad induzione impiegando la tecnica degli elementi finiti', *Proc. SIMAI '92 Conf.*, Florence 1–5 June, 1992.
8. J. Davies and P. Simpson, *Induction Heating Handbook*, McGraw-Hill, London, 1979.
9. A. Tarantola, *Inverse Problem Theory*, Elsevier, Amsterdam, 1987.
10. O. C. Zienkiewicz, W. L. Wood and N. W. Hine, 'A unified set of single step algorithms. Part 1: general formulation and applications', *Int. j. numer. methods eng.*, **20,** 1529–1552 (1984).
11. A. K. M. Ai-Shaikhli and L. Hobson, 'Novel technique for the design of induction billet heaters', *IEE Proc.*, Part B, **133,** 323–330 (1986).
12. G. Maizza, G. Mettifogo and B. Debenedetti, 'The Ansys code for the solution of induction heating problems', to be presented at 9th *Int. Conf. on Heat Treatment and Surface Engineering*, ATTT '94, Nice-Acropolis (French) 26–28 September, 1994.
13. G. Maizza, *Ph.D. Thesis*, 1995.